Magnetic properties of textured ferrocomposite consisting of immobilized superparamagnetic nanoparticles

Anna Yu. Solovyova, Ekaterina A. Elfimova, and Alexey O. Ivanov*
Department of Theoretical and Mathematical Physics, Institute of Nature Sciences and Mathematics, Ural Federal University, 51 Lenin Avenue, Ekaterinburg 620000, Russia

(Received 19 July 2021; accepted 9 December 2021; published 28 December 2021)

Wide use of magnetic nanoparticles in modern technologies and biomedical applications requires reliable theoretical models capable of predicting physical properties. Solidification of a ferroparticle suspension under the action of permanent magnetic field allows us to obtain a ferrocomposite, characterized by some orientational texture of the nanoparticle easy magnetization axes. The static magnetic response of this ferrocomposite differs from that of the parent magnetic suspension due to "freezing" of nanoparticle translational and rotational degrees of freedom. Here the superparamagnetic fluctuations of the nanoparticle magnetic moments play a key role in the formation of the ferrocomposite magnetic response depending on the degree of orientational ordering, obtained during synthesis of a ferrocomposite. With the help of statistical mechanics we calculate the magnetization and the initial magnetic susceptibility of the textured ferrocomposite for various temperatures and magnetic field strengths. The easy axis texturing leads to a significant increase of the magnetic properties, and the effect intensifies with the growth of nanoparticle magnetocrystalline anisotropy. Theoretical predictions are supported by Monte Carlo simulations. The obtained results evidence that the texturing of a ferroparticle suspension and transforming it into a textured ferrocomposite are a real way to enhance the magnetic response of these magnetic soft materials.

DOI: 10.1103/PhysRevE.104.064616

I. INTRODUCTION

So-called magnetic soft matter includes polycomponent materials consisting of magnetic particles embedded in some liquid or elastic carriers. These particles play the part of elementary magnetic units; embedding a large number of such particles into a matrix makes it possible to control the properties of a composite material using an external magnetic field [1], and it is this control which is exploited in modern technologies and biomedical applications. Examples of magnetic soft materials include ferrofluids, magnetorheological suspensions, magnetic elastomers and ferrogels, ferronematic liquid crystals, and various biocompatible magnetic suspensions.

The fundamental properties of liquid suspensions of superparamagnetic and/or ferromagnetic particles have been studied in detail experimentally [2–9] and theoretically [10–18] and in computer simulations [3,18–24]. Now both the static and dynamic magnetic properties of bulk magnetic liquids are well understood, including the effects of interparticle interactions. In such systems, whether the particles are superparamagnetic or ferromagnetic is unimportant, as long as the particles are free to rotate.

In this work, the response of weakly interacting single-domain superparamagnetic nanoparticles (SNPs) with a typical diameter ∼10 nm, immobilized in a solid matrix, to an applied magnetic field is studied using statistical mechanical theory and computer simulations. SNPs of this size are typically used in ferrofluids [1]; these particles are involved in intensive Brownian motion, which prevents particle sedimentation and provides a high colloidal stability of ferrofluids. The particles are considered to be spherical and are smaller than the minimal size of a single magnetic domain in the bulk material. Hence, a SNP should be described with the help of a core-shell model, in which each SNP contains an inner, uniformly magnetized spherical core, the magnetization of which is equal to the bulk magnetization of the material. The core is surrounded by a so-called dead magnetic layer, the presence of which can be explained by the frustration of the spin order close to the particle surface. Usually, the particles are also covered with an adsorbed layer of surfactant molecules, which provides steric stabilization against irreversible coagulation [1].

A crystalline lattice of a ferro- or ferrimagnetic material of SNPs is characterized by the presence of some axes along which the spontaneous alignment of atom spins has an energy advantage. This lattice axis is commonly called an "axis of easy magnetization" or simply an "easy axis" [25]. In the simplest case, the crystalline structure of the magnetic material has only one axis of easy magnetization (uniaxis magnetization), meaning that there is only one easy axis of spin alignment. Uniaxis anisotropy is typically used for magnetite SNPs (see, for example, [1]). The single-SNP magnetic properties are therefore controlled by the energy barrier separating the two degenerate alignments of a SNP magnetic moment with respect to its easy axis and the interaction energy between the SNP dipole and the field. Here we focus on the ferrocomposite, in which the SNPs are dispersed uniformly

*alexey.ivanov@urfu.ru

throughout the matrix while the orientations of the easy axes are subjected to texturing. The SNP's easy axes can be aligned in a liquid precursor solution using a strong magnetic field before initiating a chemical reaction of polymerization or physical process that solidifies the suspending medium. In what follows, we call this field the "polymerization field." The probing field can then be applied at any angle with respect to the polymerization field direction. The isotropic distribution of the SNP's easy axes is, of course, the default situation without any field applied during synthesis of a ferrocomposite.

The synthesis of these ferrocomposites is now a well-developed technique, as described in many experimental works [26–34]. The alignment of easy axes and the ferrocomposite physical properties were also the subject of theoretical studies [32,35–37] and computer simulations [31,37,38]. A general description of the magnetoactive composites can also be found in reviews [39,40]. Additionally, it is worth mentioning that more ordered SNP structures, such as the location of SNPs in the nodes of an ordered lattice [41,42], were studied theoretically. Liquid matrix solidification is also used in the synthesis of multicore micron-sized particles comprising several dozen or hundreds of SNPs [43–45]. The magnetic response of multicore particles is dependent on the degree of easy axes alignment [46–51]. The synthesis of the polymer beads, covered with a textured magnetic layer, is also worth mentioning [52–54].

In all the mentioned theoretical and simulation works the orientational ordering of the SNP easy axes is considered as originally given. Unlike these approaches, here we trace the dependence of the ferrocomposite magnetic properties on the orientational texturing obtained in the initial ferrofluid under the condition of the fast solidification of the liquid carrier. As a result, we calculate the magnetization and initial magnetic susceptibility of the ferrocomposite as a function of the polymerization field strength and polymerization temperature as well as a functions of magnetic field and temperature, set during magnetic measurements.

The rest of this article is organized as follows. The theoretical approach is detailed in Sec. II, including the noninteracting ferrofluid (Sec. II B), the orientation structure of the textured ferrocomposite (Sec. II C), and its static magnetic properties (Sec. II D). The Monte Carlo simulation protocol is described in Sec. III. Section IV contains the results, and Sec. V concludes the article.

II. THEORY

A. Model of a superparamagnetic nanoparticle

Let us consider the spherical single-domain SNPs suspended in some liquid or polymer solution. Each SNP has a magnetic core of diameter $x \sim 10$–15 nm and volume $v_m = \pi x^3/6$; this core is uniformly magnetized, and its magnetic material is characterized by the bulk saturation magnetization M_s and the magnetic anisotropy constant K. So the absolute value of the SNP magnetic moment is $m = M_s v_m$; we consider a uniaxial magnetocrystalline structure of the SNP material. The particles are covered with surfactant shell to prevent colloidal coagulation; thus, the SNP hydrodynamic diameter d exceeds its magnetic core size: $d = x + 2l$, where l stands for the nonmagnetic layer thickness. The SNP number concentration is ρ, and the volume fraction is $\varphi = \rho\pi d^3/6$. The center position of each ith SNP is defined by its radius vector $\mathbf{r}_i$, and the direction of the SNP easy magnetization axis is determined by the unit vector $\hat{\mathbf{n}}_i$.

For common nanosize particles, as considered before, the anisotropy energy barrier Kv_m may be comparable to the thermal energy k_BT, and so thermal fluctuations result in stochastic reorientations of the magnetic moment inside the SNP. The mean value of the SNP magnetic moment, measured over a long time, will be equal to zero. This behavior is known as Néel superparamagnetism, and it is a characteristic feature of only nanosize particles [37]. Superparamagnetic fluctuations are commonly described as the thermally activated rotations of the magnetic moment inside the SNP. Importantly, this mechanism means that even if particle positions and orientations (easy axes) are frozen, the magnetic moments are still able to rotate, subject to the potential energy U_N and the magnetic energy U_m of the interaction with an external magnetic field:

$$U_N(i) = -Kv_m(\hat{\mathbf{m}}_i \cdot \hat{\mathbf{n}}_i)^2, \tag{1}$$

$$U_m(i) = -\mu_0(\mathbf{m}_i \cdot \mathbf{H}) = -\mu_0 mH(\hat{\mathbf{m}}_i \cdot \hat{\mathbf{h}}). \tag{2}$$

Here $\hat{\mathbf{m}}_i = \mathbf{m}_i/m$ is the unit vector of the ith SNP magnetic moment orientation, μ_0 is the vacuum magnetic permeability, the applied static uniform magnetic field $\mathbf{H}$ has strength H, and the orientation $\hat{\mathbf{h}} = \mathbf{H}/H$.

In addition to volume fraction φ, two dimensionless parameters are associated with these potentials, which measure the corresponding energies with respect to the thermal energy k_BT,

$$\sigma = \frac{Kv_m}{k_BT}, \quad \alpha = \frac{\mu_0 mH}{k_BT}, \tag{3}$$

where σ is the magnetocrystalline anisotropy parameter and α is the Langevin parameter characterizing the particle-field interactions. Concerning the interparticle magnetic interaction, it should be mentioned that the characteristic energy $\mu_0 m^2/4\pi d^3$ of interaction of two magnetite (for example) SNPs with a magnetic core diameter of 10–12 nm, a bulk magnetization of magnetite of 480 kA/m, and a nonmagnetic layer thickness of 3 nm [1–3] does not exceed a value of $\sim 2 \times 10^{-21}$ J. At the same time the thermal energy at room temperatures is of the order of $\sim 4 \times 10^{-21}$ J. So we may conclude that the interparticle magnetic energy is at least two times lower than the thermal energy; thus, the interparticle interaction can be neglected.

The sample container is taken as a highly elongated cylinder aligned along the laboratory Oz axis, and the applied magnetic field $\hat{\mathbf{h}} = (0, 0, 1)$ is in the same direction. This means that demagnetization effects can be neglected, and the internal magnetic field can be taken to be the same as the external applied field H. The ith SNP radius vector is $\mathbf{r}_i = r_i(\sin\theta_i\cos\phi_i, \sin\theta_i\sin\phi_i, \cos\theta_i)$, θ_i is the polar angle with respect to the laboratory Oz axis, and ϕ_i is the azimuthal angle with respect to the laboratory Ox axis. The orientation (easy axis) of the ith SNP is the unit vector $\hat{\mathbf{n}}_i = (\sin\xi_i\cos\psi_i, \sin\xi_i\sin\psi_i, \cos\xi_i)$, where ξ_i and ψ_i are, respectively, the polar and azimuthal angles in the

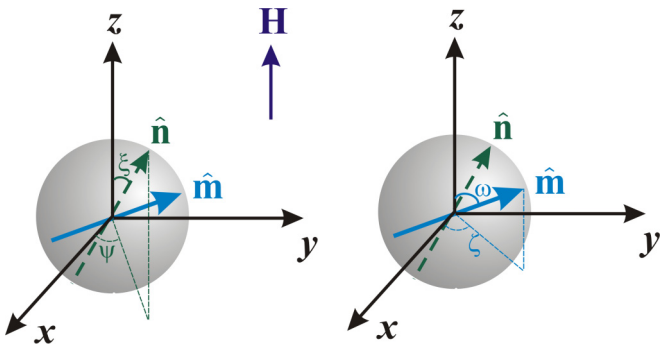

FIG. 1. Laboratory coordinate system. The orientation of the particle is given by the body-fixed, magnetic easy axis vector $\hat{\mathbf{n}} = (\sin\xi\cos\psi, \sin\xi\sin\psi, \cos\xi)$, where ξ and ψ are, respectively, the polar and azimuthal angles. The orientation of the particle magnetic moment $\hat{\mathbf{m}} = (\sin\omega\cos\zeta, \sin\omega\sin\zeta, \cos\omega)$ can be different from the easy axis vector due to superparamagnetic fluctuations (ω and ζ are, respectively, the polar and azimuthal angles).

laboratory frame. The ith SNP magnetic moment orientation is $\hat{\mathbf{m}}_i = (\sin\omega_i\cos\zeta_i, \sin\omega_i\sin\zeta_i, \cos\omega_i)$, and ω_i and ζ_i are, respectively, the polar and azimuthal angles. These vectors are shown in Fig. 1.

The described ferrofluid is magnetized in equilibrium with field strength H_p at temperature T_p, and then the SNP positions and orientations become fixed if the liquid carrier of the suspension is solidified. The possibility of quasiequilibrium transformation of a ferrofluid into a solid substance by means of carrier liquid polymerization, for example, has been experimentally verified many times [26,27,33,34]. Ferrofluid, polymerized in the presence of an external field, forms a texture, the anisotropy degree of which is a function of the polymerization field H_p and the polymerization temperature T_p. Thus, the SNPs lose their translational and rotational degrees of freedom, and the ferrofluid transforms into a textured ferrocomposite. In what follows, we describe the static magnetic properties of these immobilized SNPs at various magnetic field strengths H and temperatures T.

B. Noninteracting SNP ferrofluid

The orientation structure of a noninteracting SNP ferrofluid at a static applied magnetic field is described by the one-particle distribution density W_{FF} [35],

$$W_{FF}(\hat{\mathbf{m}}_i, \hat{\mathbf{n}}_i) = \frac{\exp\left[\sigma(\hat{\mathbf{m}}_i\cdot\hat{\mathbf{n}}_i)^2 + \alpha(\hat{\mathbf{m}}_i\cdot\hat{\mathbf{h}})\right]}{Z_{FF}(\alpha,\sigma)}, \tag{4}$$

$$Z_{FF} = \int d\hat{\mathbf{n}}_i \int d\hat{\mathbf{m}}_i \exp\left[\sigma(\hat{\mathbf{m}}_i\cdot\hat{\mathbf{n}}_i)^2 + \alpha(\hat{\mathbf{m}}_i\cdot\hat{\mathbf{h}})\right]$$

$$= \frac{\sinh\alpha}{\alpha} R(\sigma), \quad R(\sigma) = \int_0^1 \exp(\sigma t^2) dt,$$

$$\int d\hat{\mathbf{m}}_i = \frac{1}{4\pi}\int_0^{2\pi} d\zeta_i \int_{-1}^{1} d\cos\omega_i,$$

$$\int d\hat{\mathbf{n}}_i = \frac{1}{4\pi}\int_0^{2\pi} d\psi_i \int_{-1}^{1} d\cos\xi_i. \tag{5}$$

Here Z_{FF} stands for the partition function of a gas of noninteracting SNPs [10], representing the exponential Boltzmann-type distribution (4) averaged over all possible degrees of freedom, specifically here over all possible orientations of the SNP easy axes $d\hat{\mathbf{n}}_i$ and the SNP magnetic moment $d\hat{\mathbf{m}}_i$, so that $\int d\hat{\mathbf{n}}_i \cdot 1 = 1$ and $\int d\hat{\mathbf{m}}_i \cdot 1 = 1$. Obviously, the magnetization M_L of this noninteracting SNP suspension is defined as the averaged projections of the SNP magnetic moment onto the magnetic field direction:

$$M_L = \rho m \int d\hat{\mathbf{n}}_i \int d\hat{\mathbf{m}}_i (\hat{\mathbf{m}}_i\cdot\hat{\mathbf{h}}) W_{FF}(\hat{\mathbf{m}}_i, \hat{\mathbf{n}}_i)$$

$$= \rho m \frac{\partial \ln Z_{FF}}{\partial\alpha} = \rho m L(\alpha), \tag{6}$$

and it is determined by the Langevin function $L(\alpha) = \coth\alpha - 1/\alpha$. The initial magnetic susceptibility is defined by the Langevin expression $\chi_L = \mu_0\rho m^2/3k_BT$.

The orientation distribution f_{FF} of noninteracting SNP easy magnetization axes is given by function (4) averaged over only the magnetic moment direction [35,37],

$$f_{FF}(\hat{\mathbf{n}}_i) = \int d\hat{\mathbf{m}}_i W_0(\hat{\mathbf{m}}_i, \hat{\mathbf{n}}_i) = \frac{Z_{FC}(\hat{\mathbf{n}}_i, \alpha, \sigma)}{Z_{FF}(\alpha,\sigma)}, \tag{7}$$

$$Z_{FC}(\hat{\mathbf{n}}_i, \alpha, \sigma) \equiv Z_{FC}(\xi_i, \alpha, \sigma)$$

$$= \int d\hat{\mathbf{m}}_i \exp\left[\sigma(\hat{\mathbf{m}}_i\cdot\hat{\mathbf{n}}_i)^2 + \alpha(\hat{\mathbf{m}}_i\cdot\hat{\mathbf{h}})\right]$$

$$= \frac{1}{2}\int_{-1}^{1} \exp(\sigma t^2 + \alpha t\cos\xi_i)$$

$$\times I_0(\alpha\sqrt{1-t^2}\sin\xi_i) dt, \tag{8}$$

where $I_0(z)$ is the modified Bessel function of zeroth order. After integration over $d\hat{\mathbf{m}}_i$ this $\hat{\mathbf{n}}_i$ distribution appears to be dependent on only the polar angle ξ_i due to the cylindrical symmetry around the field direction. In the absence of field this function is equal to unity, which corresponds to uniform random distribution of SNP easy axes. With field strengthening, two symmetric peaks start growing at angles $\xi_i = 0$ and π, demonstrating the alignment of the SNP easy axes.

C. Orientation structure of the textured ferrocomposite

Let us consider the "rapid" solidification (or polymerization) of the ferrofluid liquid carrier at some field $\mathbf{H}_p || Oz$ (Fig. 1) and temperature T_p. By "rapid" solidification we mean here that the SNP orientational structure, created by the magnetic field $\mathbf{H}_p$, is not affected by the change in the phase state of the carrier matrix, which has lost its fluidity. For example, the fast freezing of the ferrofluid was described in Ref. [55] after cryogenic TEM images of the aggregated ferroparticles were obtained. A more detailed description of the synthesis of textured ferrocomposites can be found in Refs. [26–34].

The frozen orientation texture of the SNP easy axes is dependent on the corresponding values of the dimensionless parameters $\alpha_p = \mu_0 m H_p/k_BT_p$ and $\sigma_p = Kv_m/k_BT_p$. This fixed distribution f_p is given in accordance to expression (7),

$$f_p(\hat{\mathbf{n}}_i, \alpha_p, \sigma_p) \equiv f_p(\xi_i, \alpha_p, \sigma_p) = \frac{Z_{FC}(\xi_i, \alpha_p, \sigma_p)}{Z_{FF}(\alpha_p, \sigma_p)}. \tag{9}$$

It is worth mentioning that the ferrofluid magnetization (6) is independent of the value of magnetic anisotropy σ. At the same time, the easy axis orientation distribution (9) is a robust

function of σ_p. Obviously, an external static uniform magnetic field influences the SNP magnetic moments only orientationally. Meanwhile, expression (9) evidences the formation of the easy axis orientation texture. The physical reason for this formation is the energetic interaction between the magnetic moment and the easy magnetization axis (1). The "strength" of this interaction is controlled by the parameter σ. So the larger σ is, the more pronounced the texture is. For the case of negligibly weak magnetocrystalline anisotropy, no easy axis orientational texture can be obtained with the help of equilibrium magnetization: $f_p(\xi_i, \alpha_p, \sigma_p = 0) = 1$.

It is convenient to describe the degree of alignment of the SNP easy axes, i.e., the degree of ordering of the textured ferrocomposite, with the help of the distribution moments Q_k:

$$Q_k = \frac{1}{2}\int_{-1}^{1} f_p(\xi_i, \alpha_p, \sigma_p) P_k(\cos\xi_i) d\cos\xi_i, \qquad (10)$$

where $P_k(z)$ are the Legendre polynomials. The zero moment Q_0 stands for the simple normalization, that is, unity, $Q_0 = 1$. The first moment Q_1 has the same meaning as the magnetization, and it describes the degree of coalignment of vectors $\hat{\mathbf{n}}_i$. Obviously, Q_1 is zero at any α_p and σ_p since orientations $\pm\hat{\mathbf{n}}_i$ are equally probable.

The degree of SNP easy axis parallelism is described by the second moment Q_2, which is zero for uniform random configuration and is equal to unity for the complete parallel alignment. This moment can be calculated analytically:

$$Q_2(\alpha_p, \sigma_p) = \frac{A_\parallel(\sigma_p) - 1}{2} L_3(\alpha_p), \qquad (11)$$

where the function $L_3(z) = 1 - 3L(z)/z$ is known as the third Langevin function, $L_3(0) = 0$, $L_3(\infty) = 1$. The function

$$A_\parallel(\sigma) = 3\frac{d\ln R(\sigma)}{d\sigma} = \frac{3}{2\sigma}\left[\frac{\exp(\sigma)}{R(\sigma)} - 1\right] \qquad (12)$$

was introduced in Refs. [37,56]; it describes the initial magnetic susceptibility of immobilized SNPs, the easy axes of which are directed parallel to the field. For magnetically soft SNPs, $A_\parallel(\sigma = 0) = 1$, it increases monotonously with growing σ [51],

$$A_\parallel(\sigma) \approx 1 + \frac{4\sigma}{15} + \frac{8\sigma^2}{315} - \frac{16\sigma^3}{4725} - \frac{32\sigma^4}{31185}, \quad \sigma < 3, \qquad (13)$$

asymptotically reaching the value $A_\parallel(\sigma \to \infty) \to 3$:

$$A_\parallel(\sigma) \approx 3\left(1 - \frac{1}{\sigma} - \frac{1}{2\sigma^2}\right), \quad \sigma > 3. \qquad (14)$$

So, the second moment Q_2 is the increasing function of both α_p and σ_p.

It is worth mentioning that the maximum achievable parallelism of SNP easy axes at $\alpha_p \to \infty$ is not unity:

$$Q_2(\alpha_p \to \infty, \sigma_p) = \frac{A_\parallel(\sigma_p) - 1}{2}. \qquad (15)$$

Moreover, at low anisotropy $\sigma_p \ll 1$ the second moment is close to zero; this means that this ferrofluid cannot be textured even at the condition of magnetic saturation.

D. Textured ferrocomposite: Static magnetic properties

Now we have a sample with a textured ferrocomposite, the SNPs of which are immobilized and the easy magnetization axes of which are directed according to the orientation distribution $f_p(\xi_i, \alpha_p, \sigma_p)$ (9). The magnetic moments are still able to rotate within SNPs, and the static magnetic properties of the sample are determined by the response of single SNPs since we neglect the interparticle correlations. Here the ferrocomposite one-particle distribution density W_{FC} differs from W_{FF} (4) since the easy axis orientation is not the degree of freedom, and the normalization partition function Z_{FC} does not include the averaging over $d\hat{\mathbf{n}}_i$:

$$W_{FC}(\hat{\mathbf{m}}_i, \hat{\mathbf{n}}_i) = \frac{\exp\left[\sigma(\hat{\mathbf{m}}_i \cdot \hat{\mathbf{n}}_i)^2 + \alpha(\hat{\mathbf{m}}_i \cdot \hat{\mathbf{h}})\right]}{Z_{FC}(\hat{\mathbf{n}}_i, \alpha, \sigma)}. \qquad (16)$$

The angle $\hat{\mathbf{n}}_i$ dependence of Z_{FC} is given in Eq. (8).

Let us examine first the magnetic response to a static magnetic field H, applied along the same direction as the polymerization field H_p, $\mathbf{H}||\mathbf{H}_p$; we call it the "parallel" case. Here the magnetization $M_\parallel$ of the textured ferrocomposite is defined similarly to expression (6) but includes the orientation distribution of the SNP easy axes (9):

$$\begin{aligned} M_\parallel &= \rho m \int d\hat{\mathbf{n}}_i f_p(\xi_i, \alpha_p, \sigma_p) \int d\hat{\mathbf{m}}_i (\hat{\mathbf{m}}_i \cdot \hat{\mathbf{h}}) W_{FC}(\hat{\mathbf{m}}_i, \hat{\mathbf{n}}_i) \\ &= \frac{\rho m}{2Z_{FF}(\alpha_p, \sigma_p)} \frac{\partial}{\partial\alpha} \int_{-1}^{1} Z_{FC}(\xi, \alpha_p, \sigma_p) \\ &\quad \times \ln Z_{FC}(\xi, \alpha, \sigma)\, d\cos\xi. \end{aligned} \qquad (17)$$

The magnetization curve, described by this expression, exhibits an interesting feature in the case when parameters α and σ of the magnetization measurement coincide with α_p and σ_p of the liquid solidification. At this point both magnetizations (17) and (6) match exactly, $M_\parallel(\alpha_p, \sigma_p) = M_L(\alpha_p)$. This feature is easy to understand because the following relation holds true:

$$\int_{-1}^{1} Z_{FC}(\xi, \alpha_p, \sigma_p)\, d\cos\xi = Z_{FF}(\alpha_p, \sigma_p).$$

Although the magnetization (17) looks rather complicated and demands numerical calculations, the initial magnetic susceptibility can be calculated in a much simpler form. Using Taylor expansion of $Z_{FC}(\xi, \alpha, \sigma)$ over small values of $\alpha \ll 1$, we get [51]

$$\ln Z_{FC}(\xi, \alpha, \sigma) = \ln R(\sigma) + \frac{\alpha^2}{6}\{1 + [A_\parallel(\sigma) - 1]\} P_2(\cos\xi). \qquad (18)$$

So expression (17) transfers to

$$\begin{aligned} M_\parallel &= \chi_\parallel H, \quad \chi_\parallel \equiv \chi_\parallel(\sigma, \alpha_p, \sigma_p) \\ &= \chi_L\{1 + [A_\parallel(\sigma) - 1] Q_2(\alpha_p, \sigma_p)\}. \end{aligned} \qquad (19)$$

In the case of complete easy axis alignment ($Q_2 = 1$), we get $\chi_\parallel = \chi_L A_\parallel$ [37]. Otherwise, for the random orientation of the SNP easy axes the susceptibility is equal to the Langevin one, $\chi_\parallel = \chi_L$.

Calculating the ferrocomposite magnetic properties becomes more complicated when a magnetic field is applied

perpendicularly to H_p, $\mathbf{H} \perp \mathbf{H}_p$, for example, along the Ox axis. Ferrocomposite magnetization $M_\perp$ is also defined by expression (17), making corresponding corrections due to the field direction. But the initial magnetic susceptibility $\chi_\perp$ can be calculated in a simple form (see the Appendix):

$$M_\perp = \chi_\perp H, \quad \chi_\perp \equiv \chi_\perp(\sigma, \alpha_p, \sigma_p) = \chi_L\left\{1 - \frac{[A_\parallel(\sigma) - 1]}{2} Q_2(\alpha_p, \sigma_p)\right\}. \tag{20}$$

For the nontextured system the susceptibility evidently equals the Langevin one, $Q_2 = 0$, $\chi_\perp = \chi_\parallel = \chi_L$. For the case of complete easy axis alignment we get $Q_2 = 1$, $\chi_\perp = \chi_L(3 - A_\parallel)/2$; this result coincides with the one presented in Ref. [37] for the perpendicular texture in the system of immobilized SNPs.

Expressions (19) and (20) exhibit the interesting feature of the ferrocomposite:

$$\frac{\chi_\parallel + 2\chi_\perp}{3} = \chi_L, \tag{21}$$

independent of the presence of an orientational structure and of the strength of the internal magnetocrystalline anisotropy.

III. MONTE CARLO SIMULATIONS

To test the obtained theoretical predictions canonical (NVT) Monte Carlo simulations were carried out for an ensemble of $N = 512$ superparamagnetic dipolar hard spheres. Periodic boundary conditions were applied to a cubic box of volume V. The direction of the external magnetic field was assumed to be along the Oz axis. To model the SNP ferrofluid, three equiprobable types of moves were used: translational movement of the particle, random displacement of both the magnetic moment and easy axis at the same trial angle (Brownian rotation), and rotation of the magnetic moment regardless of the easy axis (Néel rotation). In the last case, rotations were performed using both a conventional random displacement and the flip move $\mathbf{m} \to -\mathbf{m}$ to overcome the anisotropy barrier, especially for $\sigma \gg 1$ [37]. After 10^6 attempted translations and rotations per nanoparticle, the typical run was extended by another 5×10^5 Monte Carlo steps, during which N_c independent configurations of SNP positions and orientations were saved to simulate a new system after the polymerization of the carrier fluid. Typical examples of easy axis orientations $\hat{\mathbf{n}}_i$ in the Oz direction are shown in Fig. 2 for different values of α_p and σ_p. At $\alpha_p = 1$ [Fig. 2(a)] one can see a uniform distribution of the value $\cos\xi_i$, while at $\alpha_p = 10$ [Fig. 2(b)] there is a pronounced tendency to align the easy axes almost parallel to the applied magnetic field. This effect is enhanced with increasing σ_p up to 10 [Fig. 2(c)]. For textured ferrocomposite modeling, the SNP positions and easy magnetization axes were fixed in the way described above. In this case only Néel rotation of the magnetic moment was used to perform the next Monte Carlo simulations.

The initial susceptibility $\chi_\parallel$ of the textured composite was determined from the fluctuation formula

$$\chi_\parallel = \frac{\mu_0 \langle M_z^2 \rangle}{V k_B T}, \tag{22}$$

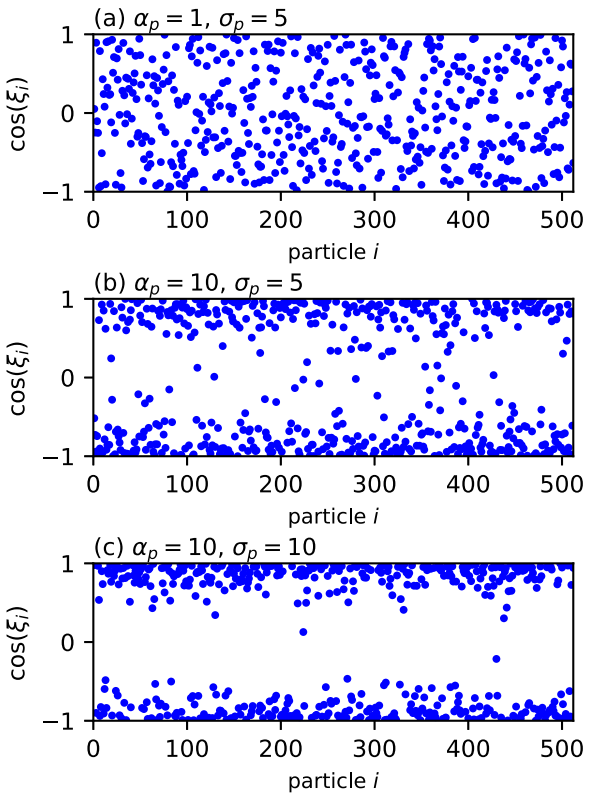

FIG. 2. The value of $\cos\xi_i$ for each particle i in the trial configuration saved during the modeling of SNP ferrofluid with $\chi_L = 1$, $\varphi = 0.125$ in an applied magnetic field: (a) $\alpha_p = 1$, $\sigma_p = 5$; (b) $\alpha_p = 10$, $\sigma_p = 5$; and (c) $\alpha_p = 10$, $\sigma_p = 10$.

where M_z is a z component of the whole magnetic moment,

$$\mathbf{M} = \sum_{i=1}^{N} \mathbf{m}_i. \tag{23}$$

Obviously, the simulation data are very "noisy" since they are dependent on the frozen displacement of SNPs at fixed α_p and σ_p. To avoid these statistical errors, for each case we average the results over the mentioned number N_c of simulations. Here there is an important question: What number N_c is sufficient to obtain the results with sufficient accuracy? To illustrate the answer we present in Fig. 3 the simulated data for the parallel susceptibility obtained for different numbers of configurations $N_c = 1$, 2, 5, 10, 20, and 30. Starting from $N_c = 5$ the results do not depend on the number of considered configurations; therefore, the value $N_c = 10$ was chosen as being optimal for computer simulations. In what follows, all simulation results were obtained within averaging over 10 independent configurations of the textured ferrocomposite for each set of system parameters α_p and σ_p. In all cases, the SNP volume concentration $\varphi = 0.125$ and the Langevin susceptibility $\chi_L = 1$ were fixed during simulations.

An example of the averaging of the angle distribution density $f_p(\xi_i)$ is shown in Fig. 4. For each configuration this function fluctuates around some basic dependence (light gray lines), the existence of which is clearly demonstrated by the averaged curves [blue (dark gray) lines]; the averaged curves have much weaker noise than the results for separate

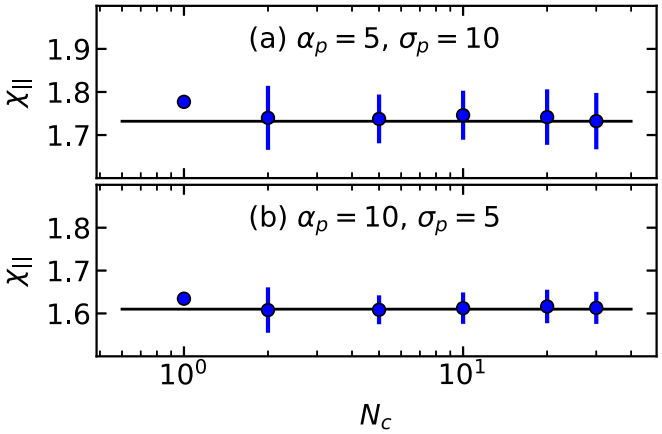

FIG. 3. The static initial magnetic susceptibility $\chi_\parallel$ of the textured ferrocomposite ($\chi_L = 1$, $\varphi = 0.125$), simulated for different numbers of configurations N_c, used for averaging the results: (a) $\alpha_p = 5$, $\sigma_p = 10$ and (b) $\alpha_p = 10$, $\sigma_p = 5$.

configurations. With increasing α_p and/or σ_p values, the difference between the results for distribution density f_p for the individual configurations decreases.

IV. RESULTS

We start with portraits of the textured ferrocomposite at various parameters α_p and σ_p of the liquid solidification. It is clear that the polymerization field strengthening leads to more pronounced orientational alignment. Typical easy axis distributions $f_p(\xi_i)$ are shown in Fig. 5. Obviously, at rather weak magnetic field [Fig. 5(a)] the orientational distribution is close to the uniform one. However, the distribution remains rather wide even at strong applied polymerization field, $\alpha_p = 10$, [Fig. 5(b)]. This value of α_p means that the ferrofluid magnetization reaches the vicinity of 90% of the magnetic

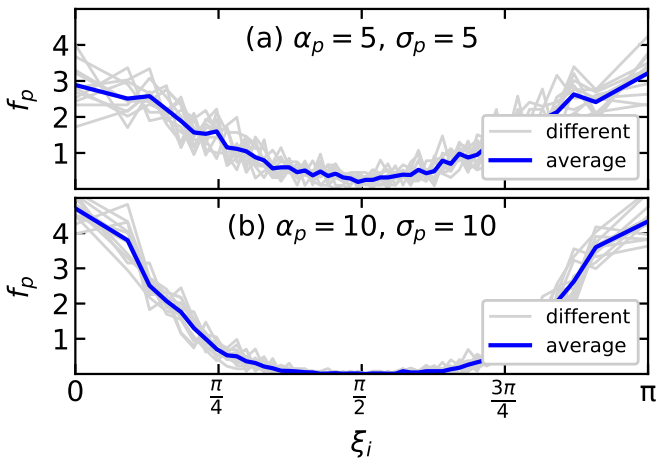

FIG. 4. The distribution density f_p of easy axes over the polar angle ξ_i for 10 configurations saved during simulations of the SNP ferrofluid with $\chi_L = 1$, $\varphi = 0.125$ in an applied magnetic field: (a) $\alpha_p = 5$, $\sigma_p = 5$ and (b) $\alpha_p = 10$, $\sigma_p = 10$. Light gray lines show the results for the 10 different configurations separately; blue (dark gray) lines represent the averaged results.

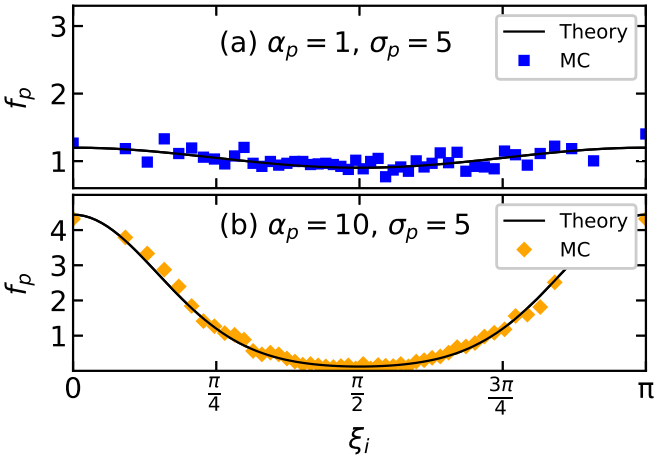

FIG. 5. The easy axis distribution f_p over the polar angle ξ_i for the textured ferrocomposite with $\chi_L = 1$, $\varphi = 0.125$, and fixed $\sigma_p = 5$. Symbols are from the MC simulations with (a) $\alpha_p = 1$ (blue squares) and (b) $\alpha_p = 10$ (orange diamonds). Theoretical predictions (9) for the same parameters are given by the solid lines.

saturation state at the solidification. At the same time, the orientational distribution is far from the δ function alignment.

Varying the polymerization value of the magnetocrystalline parameter σ_p at fixed α_p, we get qualitatively similar orientational distributions. The SNPs with a higher anisotropy barrier demonstrate a more pronounced orientational texture for the same values of the dimensionless polymerization field. This effect is demonstrated in Figs. 6(a)–6(c).

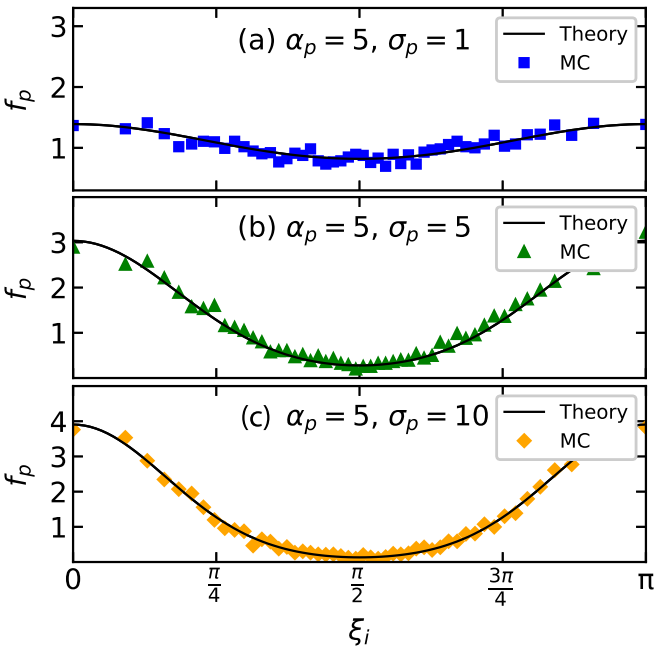

FIG. 6. The easy axis distribution f_p over the polar angle ξ_i for the textured ferrocomposite with $\chi_L = 1$, $\varphi = 0.125$, and fixed polymerization field strength $\alpha_p = 5$. Symbols are from the MC simulations with (a) $\sigma_p = 1$ (blue squares), (b) $\sigma_p = 5$ (green triangles), and (c) $\sigma_p = 10$ (orange diamonds). Solid lines present the theoretical predictions (9).

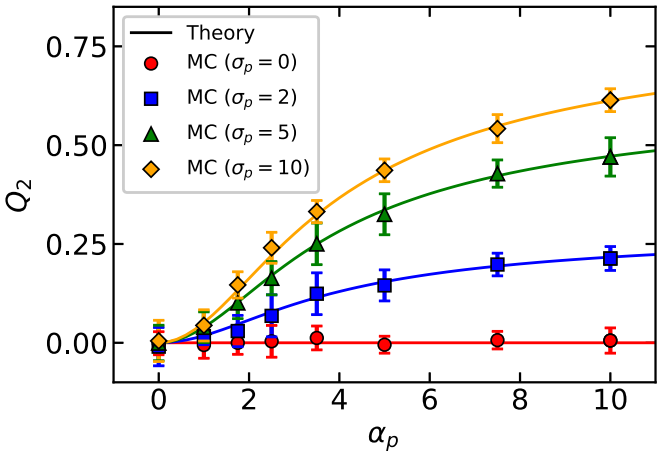

FIG. 7. The orientational distribution second moment Q_2 of the textured ferrocomposite ($\chi_L = 1,\ \varphi = 0.125, \sigma = \sigma_p$) as a function of the polymerization field α_p. Solid lines are from the theory (11); symbols are from simulations with $\sigma_p = 0$ (red circles), $\sigma_p = 2$ (blue squares), $\sigma_p = 5$ (green triangles), and $\sigma_p = 10$ (orange diamonds).

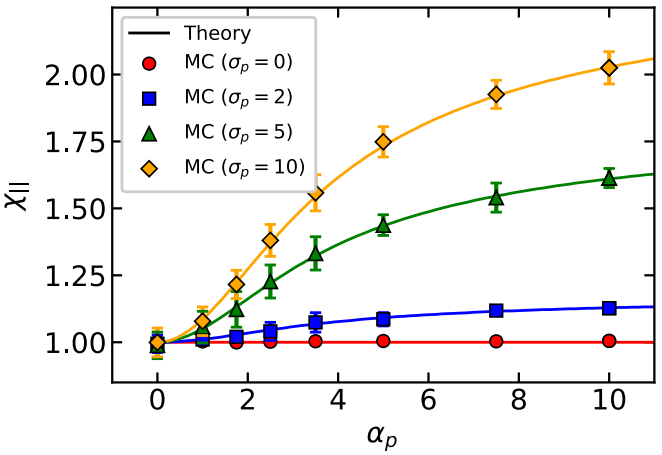

FIG. 8. The static initial magnetic susceptibility $\chi_{\|}$ of the textured ferrocomposite ($\chi_L = 1,\ \varphi = 0.125,\ \sigma = \sigma_p$) as a function of the polymerization field α_p. Solid lines are from the theory (19); symbols are from simulations with $\sigma_p = 0$ (red circles), $\sigma_p = 2$ (blue squares), $\sigma_p = 5$ (green triangles), and $\sigma_p = 10$ (orange diamonds).

It is worth mentioning here that the simulation data look rather noisy, especially in the cases in Figs. 5(a) and 6(a), where the orientation texture is not expressed well. Presumably, more accurate data demand a larger number of particles in the simulation box and a larger number of configurations over which the averaging is to be performed. Despite fluctuating data on orientation distribution density, the mean characteristics appear to be rather smooth, like the second moment Q_2, shown in Fig. 7 as a function of dimensionless field strength α_p, applied during liquid solidification, for various values of the anisotropy parameter σ_p. Clearly, negligibly weak anisotropy ($\sigma_p = 0$) allows magnetic moments to rotate freely inside SNPs, and so no SNP body oriented texture is formed at any applied field. The stronger the anisotropy is, the more pronounced the effect of the orientational texturing is. But the second moment is far from unity even for a very high anisotropy barrier and rather strong polymerization field, $\sigma_p = 10,\ \alpha_p = 10$. This means that the orientational easy axis structure cannot be considered perfectly coaligned for the really achievable SNPs parameters.

At the same time the textured ferrocomposite demonstrates much stronger static magnetic response in comparison with the ferrofluid, characterized by the same physical parameters as the ferrocomposite. This effect is most strongly manifested in the static parallel initial magnetic susceptibility $\chi_{\|}$, whose the dependence on the polymerization field strength is presented in Fig. 8 for various values of the anisotropy parameter. The susceptibility, simulated using expression (22), is given by the symbols, and the theoretical predictions (19) are shown by solid lines. In both Figs. 7 and 8, we show only the case when the temperature T coincides with the temperature T_p of the liquid solidification; this means that σ coincides with σ_p. Obviously, the temperature decrease results in an increase of the susceptibility in comparison with the one shown in Fig. 8.

Formation of the orientational texture appears to influence strongly the parallel susceptibility. For example, the values $\sigma_p = 5,\ \alpha_p = 5$ are not accompanied by well-developed easy axes coalignment, as shown in Fig. 6(b). But the ferrocomposite parallel susceptibility exceeds the ideal paramagnetic gas Langevin susceptibility by 50% (see the green triangles in Fig. 8). The largest simulated coalignment, achieved for $\sigma_p = 10,\ \alpha_p = 10$ in Fig. 7, is only $Q_2 = 0.62$. At the same time, this nonperfect orientation structure results in two time increase of the parallel susceptibility (see Fig. 8, orange diamonds).

Equilibrium magnetization curves of the ferrocomposite were simulated on the basis of described method for the parallel geometry using expression (23), and the theoretical magnetization (17) was calculated numerically. Both magnetization curves are shown in Fig. 9 in comparison with the ferrofluid magnetization curve. Four ferrocomposite structures are investigated; they were simulated with different pairs of polymerization parameters $(\sigma_p, \alpha_p) = (5, 5), (5, 10), (10, 5), (10, 10)$. For each pair (each ferrocomposite sample) the magnetization curves $M_{\|}(\alpha)$ were simulated for 10 different configurations of particle displacement and easy axis orientations. The results were averaged over these 10 simulation variants, and the averaged data are shown in Fig. 9. Evidently, in weak field the magnetization curve of the textured ferrocomposite grows with the field strength more rapidly than the ferrofluid magnetization, shown in black. At the coincidence point of an applied field with the polymerization field, $\alpha = \alpha_p$, the magnetization curves cross each other. In stronger fields the ferrocomposite reaches the magnetic saturation slower than the ferrofluid. This effect, discussed theoretically in Sec. II D, is clearly seen in Fig. 9, and it appears to be more pronounced for SNPs with higher values of the magnetocrystalline anisotropy barrier.

V. CONCLUSION

The magnetic properties of a textured ferrocomposite consisting of immobilized SNPs were described here for the case of weakly interacting SNPs under the condition the interparticle magnetic interaction can be neglected. Unlike known theoretical models, developed for the ideal alignment of the

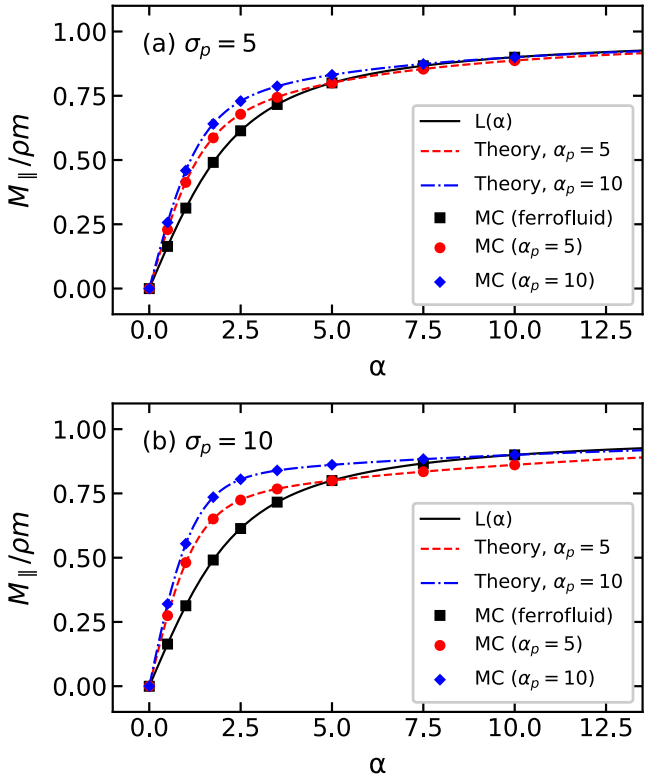

FIG. 9. The magnetization $M_\parallel$ as a function of the dimensionless magnetic field, expressed in Langevin units α, for both a ferrofluid and ferrocomposite with $\chi_L = 1$, $\varphi = 0.125$, and (a) $\sigma_p = 5$ and (b) $\sigma_p = 10$. The ferrofluid magnetization curves are given by black squares and black solid lines. The magnetization curves for the textured ferrocomposite are shown for two values of the polymerization field: $\alpha_p = 5$ (dashed lines and red circles) and $\alpha_p = 10$ (dot-dashed lines and blue diamonds). Theoretical magnetization curves (17) were calculated numerically.

SNP easy magnetization axes, for example, the one in [37], we consider a more realistic situation in which the textured ferrocomposite is obtained after fast solidification (or polymerization) of the ferrofluid liquid matrix at some temperature in the presence of an external permanent magnetic field (polymerization field). During this solidification some equilibrium distribution of the SNP easy axes is established as a result of the balance between the Zeeman magnetic moment–magnetic field interaction energy and the thermal energy (thermal fluctuations). We suppose that the SNP positions and orientations become fixed after solidification of the matrix, but the SNP magnetic moments are still able to rotate inside the SNP bodies due to superparamagnetic fluctuations. Texturing of the composite means that there is a highlighted line along which the SNP axes are mainly directed. Since the SNPs lose the rotational degrees of freedom as structural units, the application of a static magnetic field results in a different magnetic response of the ferrocomposite in comparison with the initial ferrofluid.

In the present paper we studied the described effect theoretically by means of equilibrium statistical mechanics. First, we calculated the orientation probability density of the SNP easy magnetization axes in the initial ferrofluid at some polymerization temperature and some polymerization field strength. This orientational distribution is defined in (7) as the Boltzmann probability density for the randomly chosen SNP, averaged over the magnetic moment rotational degrees of freedom. Next, we used this orientational density as the characteristic of the ferrocomposite texture (9), and we calculated the magnetization of the sample of this ferrocomposite and its initial static magnetic susceptibility. Finally, simple analytical expressions for the susceptibility were obtained for two geometries: (i) the parallel case (19), in which a magnetic field is applied parallel to the direction of the polymerization field, and (ii) the perpendicular case (20), in which an applied magnetic field is turned by 90°.

We showed that realistic values of the ferrofluid SNP parameters and strengths of the polymerization field demonstrate a rather low level of alignment of the SNP easy axes in a textured ferrocomposite. This is best seen from the data on the second moment (11), the values of which are far from unity (Fig. 7), which corresponds to absolutely perfect alignment. Despite poor alignment the effect on the magnetic susceptibility appears to be rather strong. Due to even poor texture the parallel susceptibility of the ferrocomposite can be doubled (Fig. 8) compared to the initial ferrofluid susceptibility. Obviously, the present results can be applied to rather small nanoparticles, the interparticle magnetic interaction between which is very weak. But, of course, the interactions play an important part, especially for concentrated magnetic suspensions. The magnetic response of interacting SNPs, both static and dynamic, is stronger than for noninteracting ones; this effect was discovered experimentally [2,3,8,9], substantiated by means of computer simulations [19–21,23], and justified theoretically [12,13,37,48,49]. This means that the effect of enhancing the magnetic response due to the formation of texture, as discussed in the present paper, will be even more pronounced in the textured composite of interacting SNPs.

To support the obtained theoretical results and to validate the analytical expressions we performed Monte Carlo simulations, averaging the data over several microstructural configurations of SNP positions and easy axis orientations, equilibrated in the presence of a polymerization field. We get very accurate quantitative agreement between theory and simulations for the case of weakly interacting SNPs.

Thus, our results show that the texturing of a ferrofluid and transforming it into a textured ferrocomposite is a real way to significantly enhance the static magnetic response of these magnetic soft materials.

ACKNOWLEDGMENTS

The research funding from the Ministry of Science and Higher Education of the Russian Federation (Ural Federal University project within the Priority-2030 Program) is gratefully acknowledged.

APPENDIX

We present here an analytical calculation of the initial magnetic susceptibility for the case when a magnetic field is applied perpendicularly to H_p, $\mathbf{H} \perp \mathbf{H}_p$, for example, along the Ox axis.

Let us consider the ferrocomposite sample, solidified in the presence of field $\mathbf{H}_p||Oz$. After liquid carrier solidification this field is switched off, and the textured ferrocomposite sample is placed in a uniform constant magnetic field, directed along the Ox axis of the laboratory coordinate system (Fig. 1). The magnetization is defined as

$$M_\perp = \rho m \int d\hat{\mathbf{n}} f_p(\hat{\mathbf{n}}, \alpha_p, \sigma_p) \frac{\partial \ln Z_{FC}(\hat{\mathbf{n}}, \alpha, \sigma)}{\partial \alpha}. \tag{A1}$$

Paying attention to the field geometry, it is convenient to write the function Z_{FC} here in the following form:

$$Z_{FC} = \frac{1}{2}\int_{-1}^{1} \exp[\sigma t^2 + \alpha t(\hat{\mathbf{n}}\cdot\hat{\mathbf{x}})] I_0[\alpha\sqrt{1-t^2}\sqrt{1-(\hat{\mathbf{n}}\cdot\hat{\mathbf{x}})^2}]dt, \tag{A2}$$

where $\hat{\mathbf{x}}$ stands for the unit Ox-axis vector and $(\hat{\mathbf{n}}\cdot\hat{\mathbf{x}}) = \sin\xi\cos\psi$ (see Fig. 1). Expansion in a Taylor series over small $\alpha \ll 1$ within quadratic accuracy results in

$$Z_{FC} \approx \frac{1}{2}\int_{-1}^{1} \exp(\sigma t^2)\left\{1 + \frac{\alpha^2}{4}[1-(\hat{\mathbf{n}}\cdot\hat{\mathbf{x}})^2] + \frac{\alpha^2 t^2}{4}[3(\hat{\mathbf{n}}\cdot\hat{\mathbf{x}})^2 - 1]\right\}dt.$$

Thus,

$$\begin{aligned}\frac{\partial \ln Z_{FC}(\hat{\mathbf{n}}, \alpha, \sigma)}{\partial \alpha} &= \frac{\partial}{\partial \alpha}\ln\left\{R(\sigma) + \frac{\alpha^2}{4}R(\sigma)[1-(\hat{\mathbf{n}}\cdot\hat{\mathbf{x}})^2] + \frac{\alpha^2}{12}R(\sigma)A_\parallel(\sigma)[3(\hat{\mathbf{n}}\cdot\hat{\mathbf{x}})^2 - 1]\right\} \\ &= \frac{\alpha}{2}\left\{1 - \frac{A_\parallel(\sigma)}{3} + (\hat{\mathbf{n}}\cdot\hat{\mathbf{x}})^2[A_\parallel(\sigma) - 1]\right\}. \end{aligned} \tag{A3}$$

Introducing this expression in Eq. (A1), we meet with integration over $d\psi$ [$d\hat{\mathbf{n}} = (4\pi)^{-1}d\psi\, d\cos\xi$]. Since f_p is dependent on only the angle ξ, we may integrate the last term in brackets over $d\psi$ independent of f_p:

$$\frac{\alpha}{2}\int_0^{2\pi}\left\{1 - \frac{A_\parallel(\sigma)}{3} + (\hat{\mathbf{n}}\cdot\hat{\mathbf{x}})^2[A_\parallel(\sigma) - 1]\right\}d\psi = \frac{\alpha}{3}\left\{1 + \frac{[A_\parallel(\sigma) - 1]}{2}P_2(\cos\xi)\right\}.$$

Finally, we get for the initial slope of the perpendicular magnetization

$$M_\perp = \frac{\rho m \alpha}{6}\int_{-1}^{1} f_p(\xi, \alpha_p, \sigma_p)\left\{1 + \frac{[A_\parallel(\sigma) - 1]}{2}P_2(\cos\xi)\right\}d\cos\xi = \chi_\perp H, \tag{A4}$$

$$\chi_\perp = \chi_L\left\{1 - \frac{[A_\parallel(\sigma) - 1]}{2}Q_2(\alpha_p, \sigma_p)\right\}. \tag{A5}$$

[1] R. E. Rosensweig, *Ferrohydrodynamics* (Courier Corporation, North Chelmsford, MA, 2013).

[2] M. Shliomis, A. Pshenichnikov, K. Morozov, and I. Shurubor, J. Magn. Magn. Mater. **85**, 40 (1990).

[3] A. O. Ivanov, S. S. Kantorovich, E. N. Reznikov, C. Holm, A. F. Pshenichnikov, A. V. Lebedev, A. Chremos, and P. J. Camp, Phys. Rev. E **75**, 061405 (2007).

[4] K. M. Krishnan, IEEE Trans. Magn. **46**, 2523 (2010).

[5] J. M. Laskar, J. Philip, and B. Raj, Phys. Rev. E **82**, 021402 (2010).

[6] L. J. Felicia and J. Philip, Phys. Rev. E **89**, 022310 (2014).

[7] M. T. Lopez-Lopez, F. Nogueras-Lara, L. Rodriguez-Arco, N. Guigo, N. Sbirrazzuoli, A. Y. Zubarev, S. Lacis, and P. Kuzhir, Phys. Rev. E **96**, 062604 (2017).

[8] A. V. Lebedev, V. I. Stepanov, A. A. Kuznetsov, A. O. Ivanov, and A. F. Pshenichnikov, Phys. Rev. E **100**, 032605 (2019).

[9] Y. Dikansky, A. Ispiryan, I. Arefyev, and S. Kunikin, Eur. Phys. J. E **44**, 2 (2021).

[10] Y. Raikher and M. Shliomis, Soviet Physics-JETP **40**, 526 (1975).

[11] K. I. Morozov and M. I. Shliomis, J. Phys.: Condens. Matter **16**, 3807 (2004).

[12] A. O. Ivanov and O. B. Kuznetsova, Colloid J. **68**, 430 (2006).

[13] K. I. Morozov, J. Chem. Phys. **126**, 194506 (2007).

[14] J. Jordanovic and S. H. L. Klapp, Phys. Rev. E **79**, 021405 (2009).

[15] S. M. Cattes, S. H. L. Klapp, and M. Schoen, Phys. Rev. E **91**, 052127 (2015).

[16] A. Y. Solovyova, E. A. Elfimova, A. O. Ivanov, and P. J. Camp, Phys. Rev. E **96**, 052609 (2017).

[17] T. M. Batrudinov, Y. E. Nekhoroshkova, E. I. Paramonov, V. S. Zverev, E. A. Elfimova, A. O. Ivanov, and P. J. Camp, Phys. Rev. E **98**, 052602 (2018).

[18] A. O. Ivanov and P. J. Camp, Phys. Rev. E **98**, 050602(R) (2018).

[19] Z. Wang, C. Holm, and H. W. Müller, Phys. Rev. E **66**, 021405 (2002).

[20] J. O. Sindt, P. J. Camp, S. S. Kantorovich, E. A. Elfimova, and A. O. Ivanov, Phys. Rev. E **93**, 063117 (2016).
[21] A. A. Kuznetsov and A. F. Pshenichnikov, Phys. Rev. E **95**, 032609 (2017).
[22] P. Ilg and A. E. A. S. Evangelopoulos, Phys. Rev. E **97**, 032610 (2018).
[23] P. Ilg, Phys. Rev. E **100**, 022608 (2019).
[24] A. B. Dobroserdova and S. S. Kantorovich, Phys. Rev. E **103**, 012612 (2021).
[25] S. Chikazumi and C. D. Graham, *Physics of Ferromagnetism (International Series of Monographs on Physics, 94)*, 2nd ed. (Oxford University Press, 2009).
[26] G. Filipcsei, I. Csetneki, A. Szil'agyi, and M. Zr'inyi, Adv. Polym. Sci. **206**, 137 (2007).
[27] S. Abramchuk, E. Kramarenko, G. Stepanov, L. Nikitin, G. Filipcsei, A. Khokhlov, and M. Zr'anyi, Polym. Adv. Technol. **18**, 883 (2007).
[28] D. Eberbeck, F. Wiekhorst, S. Wagner, and L. Trahms, Appl. Phys. Lett. **98**, 182502 (2011).
[29] T. Yoshida, N. B. Othman, T. Tsubaki, J. Takamiya, and K. Enpuku, IEEE Trans. Magn. **48**, 3788 (2012).
[30] K. Enpuku, Y. Ueoka, T. Sakakibara, M. Ura, T. Yoshida, T. Mizoguchi, and A. Kandori, Appl. Phys. Express **7**, 097001 (2014).
[31] S. A. Shah, D. B. Reeves, R. M. Ferguson, J. B. Weaver, and K. M. Krishnan, Phys. Rev. B **92**, 094438 (2015).
[32] T. Yoshida, Y. Matsugi, N. Tsujimura, T. Sasayama, K. Enpuku, T. Viereck, M. Schilling, and F. Ludwig, J. Magn. Magn. Mater. **427**, 162 (2017).
[33] M. Deuflhard, D. Eberbeck, P. Hietschold, N. Wilharm, M. Mühlberger, R. Friedrich, C. Alexiou, and S. Mayr, Phys. Chem. Chem. Phys. **21**, 14654 (2019).
[34] S. Ikhaddalene, F. Zibouche, A. Ponton, A. Irekti, and F. Carn, Period. Polytech. Chem. Eng. **65**, 378 (2021).
[35] Y. Raikher, J. Magn. Magn. Mater. **39**, 11 (1983).
[36] A. Y. Zubarev, Phys. Rev. E **98**, 032610 (2018).
[37] E. A. Elfimova, A. O. Ivanov, and P. J. Camp, Nanoscale **11**, 21834 (2019).
[38] P. Kreissl, C. Holm, and R. Weeber, Soft Matter **17**, 174 (2021).
[39] A. M. Menzel, Phys. Rep. **554**, 1 (2015).
[40] S. Wu, W. Hu, Q. Ze, M. Sitti, and R. Zhao, Multifunct. Mater. **3**, 042003 (2020).
[41] S. Goh, R. Wittmann, A. M. Menzel, and H. Lawen, Phys. Rev. E **100**, 012605 (2019).
[42] A. Solovyova, S. Sokolsky, E. Elfimova, and A. Ivanov, J. Nanopart. Res. **23**, 139 (2021).
[43] H. Kratz, M. Taupitz, A. De Schellenberger, O. Kosch, D. Eberbeck, S. Wagner, L. Trahms, B. Hamm, and J. Schnorr, PLoS One **13**, e0190214 (2018).
[44] V. Socoliuc, D. Peddis, V. I. Petrenko, M. V. Avdeev, D. Susan-Resiga, T. Szabó, R. Turcu, E. Tombácz, and L. Vékás, Magnetochemistry **6**, 2 (2020).
[45] H. Kratz, A. Mohtashamdolatshahi, D. Eberbeck, O. Kosch, F. Wiekhorst, M. Taupitz, B. Hamm, N. Stolzenburg, and J. Schnorr, Nanomaterials **11**, 1532 (2021).
[46] F. Ahrentorp, A. Astalan, J. Blomgren, C. Jonasson, E. Wetterskog, P. Svedlindh, A. Lak, F. Ludwig, L. J. van IJzendoorn, F. Westphal, C. Grüttner, N. Gehrke, S. Gustafsson, E. Olsson, and C. Johansson, J. Magn. Magn. Mater. **380**, 221 (2015).
[47] J. Dieckhoff, D. Eberbeck, M. Schilling, and F. Ludwig, J. Appl. Phys. **119**, 043903 (2016).
[48] P. Ilg, Phys. Rev. B **95**, 214427 (2017).
[49] A. A. Kuznetsov, Phys. Rev. B **98**, 144418 (2018).
[50] T. Kahmann and F. Ludwig, J. Appl. Phys. **127**, 233901 (2020).
[51] A. O. Ivanov and F. Ludwig, Phys. Rev. E **102**, 032603 (2020).
[52] H. Singh, P. E. Laibinis, and T. A. Hatton, Langmuir **21**, 11500 (2005).
[53] H. Singh and T. A. Hatton, J. Magn. Magn. Mater. **315**, 53 (2007).
[54] T. Isojima, S. K. Suh, J. B. V. Sande, and T. A. Hatton, Langmuir **25**, 8292 (2009).
[55] M. Klokkenburg, B. H. Erné, V. Mendelev, and A. O. Ivanov, J. Phys.: Condens. Matter **20**, 204113 (2008).
[56] A. Ivanov and E. Elfimova, Magnetohydrodynamics **55**, 59 (2019).